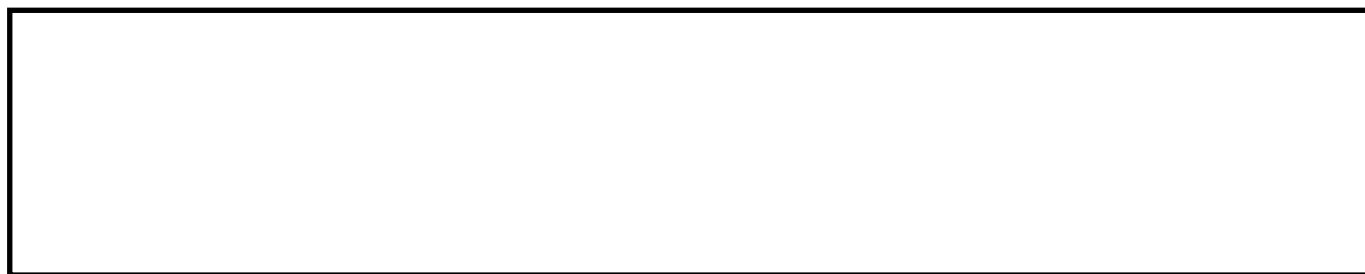


QIAO, J., WANG, S., YU, C., YANG, X. and FERNANDEZ, C. 2022. A chaotic firefly-particle filtering method of dynamic migration modeling for the state-of-charge and state-of-health co-estimation of a lithium-ion battery performance. *Energy* [online], 263(Part E), article 126164. Available from: <https://doi.org/10.1016/j.energy.2022.126164>

A chaotic firefly-particle filtering method of dynamic migration modeling for the state-of-charge and state-of-health co-estimation of a lithium-ion battery performance.

QIAO, J., WANG, S., YU, C., YANG, X. and FERNANDEZ, C.

2022



A chaotic firefly - particle filtering method of dynamic migration modeling for the state-of-charge and state-of-health co-estimation of a lithium-ion battery performance

Jialu Qiao^{a,b}, Shunli Wang^{a*,b}, Chunmei Yu^{a,b}, Xiao Yang^{a,b}, Carlos Fernandez^c

^a*School of Information Engineering, Southwest University of Science and Technology, Mianyang 621010,*

China; ^b*College of Electrical Engineering, Sichuan University, Chengdu 610065, China;* ^c*School of*

Pharmacy and Life Sciences, Robert Gordon University, Aberdeen AB10-7GJ, UK.

Abstract: In this research, a novel dynamic migration model is proposed, which can better describe the dynamic characteristics of the lithium-ion batteries under different aging states by adjusting the battery parameters in real-time. A novel chaotic firefly - particle filtering method is proposed, which realizes particle optimization by simulating the behavior of fireflies in nature attracting each other through light, and finds a new optimal solution by chaotic mapping a group of particles to different solution space, to realize high-precision state-of-charge and state-of-health co-estimation. Compared with the traditional particle filtering algorithm, the state-of-charge and state-of-health estimation accuracy of the proposed algorithm under the Hybrid Pulse Power Characterization condition is improved by 1.48% and 0.38% respectively, and that under the Beijing bus dynamic stress test condition is improved by 0.67% and 0.63% respectively. The proposed novel battery model and algorithm are of great significance in improving the condition monitoring quality of the battery management system.

Key words: electric vehicle; lithium-ion battery; state-of-charge; state-of-health; chaotic firefly; migration

1. Introduction

With the development of high-efficiency energy storage system technology and the improvement of renewable energy utilization [1, 2], new energy vehicle technology has gradually become an important way to alleviate the oil crisis and environmental pollution caused by the use of fuel vehicles [3-5]. The lithium-ion battery has the advantages of long service life [6], low self-discharge rate, and large specific energy [7], which has become the main energy source of pure electric vehicles in the driving process.

To avoid the potential safety hazards caused by lithium-ion batteries during vehicle driving [8, 9], it is necessary to efficiently manage and control lithium-ion batteries through the battery management system (BMS) [10]. As a

1
2 core parameter in the BMS [11], the state-of-charge (SOC) of the battery reflects the current remaining battery
3 level [12, 13]. In [14], the author mentioned that the SOC in electric vehicles is equivalent to the odometer of
4 traditional fuel vehicles, which can provide accurate remaining mileage for drivers. Its high-precision prediction
5 can effectively prevent the potential safety hazards caused by overcharge and over-discharge of the power batteries
6
7 [15, 16]. State-of-health (SOH) is an important parameter to describe the degree of battery aging [17], which
8 provides battery life reference for pure electric vehicles and avoids the danger caused by battery abuse during
9 vehicle driving.

10 SOC is defined as the ratio of the remaining capacity of the battery to the maximum available capacity [18-20].
11
12 At present, the estimation methods of battery SOC can be divided into the direct measurement method [21],
13 model-based method, and data-driven method [22]. Ampere-hour (Ah) method and open-circuit voltage (OCV)
14 method are common direct measurement methods [23]. Ah heavily depends on the initial SOC value and the error
15 is easy to accumulate [24, 25]. The battery is required to stand for a long time in the OCV method [26], so it is
16 not suitable for actual working conditions [27]. The data-driven method requires a large number of test samples
17 and time costs [28], while the model-based method is the most commonly used and efficient SOC estimation
18 method [29]. The core idea of the model-based estimation method is to use a mathematical model to describe the
19 relationship between state parameters and external characteristics of the battery [30-33]. However, the function
20 expression between the battery parameters and SOC of the equivalent model is usually fixed, which cannot
21 dynamically reflect the parameter changes of the battery under different aging degrees, so the single battery model
22 does not have the ability of correction [34], it needs to be combined with filtering algorithms to realize the closed-
23 loop correction of the battery model [35-37]. In [38], the OCV-SOC model based on fractional order was proposed,
24 which can better describe the strong nonlinear relationship between OCV and SOC, but it cannot meet the
25 adaptability to different aging degrees of lithium-ion batteries. In [39], the two kinds of cubature Kalman
26 filters were combined to solve the problem of inaccurate SOC initial value setting, but the overall SOC estimation
27
28
29
30
31
32
33
34
35
36
37
38
39
40
41
42
43
44
45
46
47
48
49
50
51
52
53
54
55
56
57
58
59
60
61
62
63
64
65

accuracy needs to be improved.

1
2 SOH is defined as the ratio of the current actual measured capacity to the nominal rated capacity. The research
3
4 on its estimation methods is mainly based on models and data-driven. In [40], the gaussian process regression
5
6 model which can dynamically describe the degradation characteristics of the battery was proposed. However, it is
7
8 a single state estimation method, which can only estimate SOH effectively. In [41], an independent battery
9
10 degradation modeling method was proposed to estimate SOH. It can better simulate the aging characteristics of
11
12 batteries under different working conditions, but it can not realize dynamic tracking. In [42], the combination of
13
14 parameter filter and state filter was used to form a dual Kalman filter to realize the cooperative estimation of SOC
15
16 and SOH. Although the mutual correction of two parameters was realized, the filter can only realize the estimation
17
18 in a fixed state and cannot be dynamically adjusted with the working conditions. In [43], an adaptive sliding
19
20 observer is developed to estimate the SOC and capacity, an adaptive SOH estimation scheme is proposed to
21
22 mitigate the temperature variation effect on the accuracy of the SOH estimation. The experimental results verify
23
24 the effectiveness of the proposed the adaptive sliding observer on achieving accurate estimation of SOC and
25
26 capacity. The study realized the co-estimation of SOC and SOH, and considered the influence of temperature, but
27
28 not aging.
29
30
31
32
33
34
35
36
37
38
39

40 In this research, a novel chaotic firefly - particle filtering (CF - PF) method is proposed for the SOC and SOH
41
42 co-estimation of lithium-ion batteries, which effectively solves the defects of particle degradation and particle
43
44 diversity reduction in the traditional particle filtering (PF) algorithm. PF and extended Kalman filtering (EKF) are
45
46 combined to form a dual filter to realize the mutual correction and mutual promotion of SOC and SOH. A novel
47
48 battery migration model is proposed to complete the dynamic adjustment of battery parameters with aging, which
49
50 can greatly improve the modeling accuracy and co-estimation accuracy.
51
52
53
54
55
56

57 The main contents of this paper are as follows: In the Chapter 2, mathematical analysis part is introduced. Among
58
59 them, Section 2.1 is about the construction of battery migration model, Section 2.2 is about parameter
60
61
62
63
64
65

identification, and Section 2.3 is about the SOC and SOH co-estimation by chaotic firefly - particle filtering algorithm. In the Chapter 3, experimental analysis part is introduced. It includes the establishment of the experimental platform, the verification of the migration model effect and the verification of the proposed algorithm under different working conditions. The Chapter 4 makes the conclusion of this research.

2. Mathematical analysis

Firstly, accurate modeling and model parameter identification should be carried out to characterize the dynamic characteristics of the battery. Secondly, the proposed filtering algorithm should be combined with the model, and the covariance between the observed and predicted values of battery state parameters at the previous time should be used to modify the state value at the current time, to obtain the optimal SOC and SOH co-estimation at the current time.

2.1. *Dynamic migration battery modeling*

As a highly nonlinear system, lithium-ion battery not only has complex internal electrochemical reaction but also is easily affected by ambient temperature and aging in practical application. Although the existing BMS has the temperature control function of the battery pack, which can greatly reduce the impact of ambient temperature, the impact of battery aging always runs through the normal use of the battery. Therefore, battery aging has become an important uncertain factor affecting the normal use of batteries in practical applications.

The concept of the migration battery model is different from the traditional aging battery modeling. In the traditional modeling process, the influence of battery aging is always regarded as the determining factor in the model, that is, the parameters of the battery model under different aging states are identified through multiple groups of battery experimental data under different aging states. In the battery migration modeling process, the impact of battery aging is always regarded as an uncertain factor. By combining the offline initial model part with the online migration model part, the establishment of a dynamic migration battery model can be completed by using only a small amount of experimental data in the initial state of the battery and online data in the actual use

process of the battery.

To build a lithium-ion battery model that can accurately describe different aging states, in this research, the battery equivalent circuit Thevenin model is established as the initial model, and the dynamic migration model is formed based on it, as shown in Fig. 1.

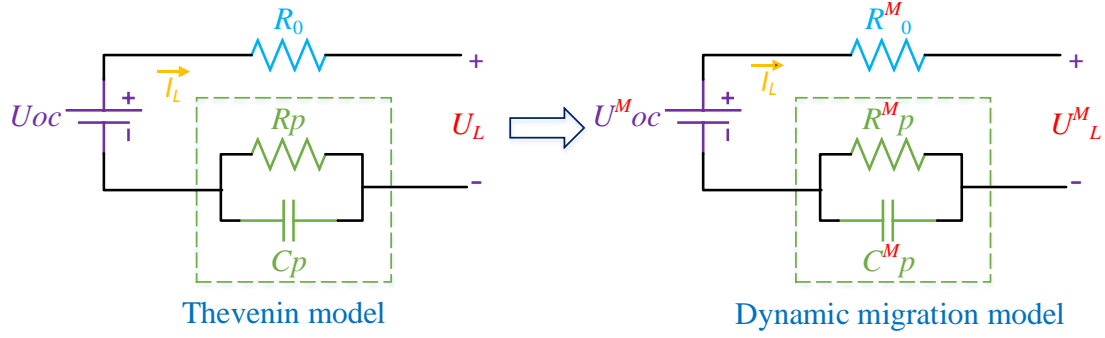


Fig. 1 Dynamic migration battery modeling

In Fig. 1, the Thevenin model consists of a voltage source, an internal resistance, and a group of parallel resistance-capacitance (RC) rings connected in series. U_{OC} is the open-circuit voltage, and R_0 represents the ohmic internal resistance inside the battery, which is formed by the resistance of the internal material of the battery itself and the contact between materials. R_p is the polarization resistance, C_p is the polarization capacitance, and the parallel circuit of R_p and C_p describes the polarization process inside the battery. U_L is the closed-circuit voltage after the battery is connected with the external circuit, and U_p is the voltage at the $R_p C_p$ terminal. The state space equation and observation equation of SOC and SOH co-estimation based on the Thevenin model is obtained, as shown in Eq. (1).

$$\begin{cases} SOC_{k+1} = SOC_k - \frac{\Delta T}{Q_k} I_k + w_{1,k} \\ U_{p,k+1} = e^{-\frac{\Delta T}{\tau}} U_{p,k} + R_p \left(1 - e^{-\frac{\Delta T}{\tau}} \right) I_k + w_{2,k} \\ Q_{k+1} = Q_k + r_k \\ U_{L,k+1} = U_{OC,k+1} - U_{p,k+1} - IR_0 + v_k \end{cases} \quad (1)$$

In Eq. (1), $[SOC \ U_p]^T$ is set as the state variable, and ΔT is the sampling time, which is set to 0.1. τ is the time

constant, $\tau = R_p C_p$. $w_{1,k}$ and $w_{2,k}$ represent process noise in SOC estimation and polarization voltage estimation, respectively. r_k represents process noise in SOH estimation, v_k represents observation noise. Q_k is the current actual capacity of the battery, which should be measured through the capacity calibration experiment. k represents the current time point, and $k + 1$ represents the next time point. The coefficient matrices of the state space equation and observation equation are shown in Eq. (2).

$$\begin{cases} A_k^{SOC} = \begin{bmatrix} 1 & 0 \\ 0 & e^{-\Delta T/\tau} \end{bmatrix} \\ B_k^{SOC} = \begin{bmatrix} -\Delta t \\ Q_k \\ R_p(1 - e^{-\Delta T/\tau}) \end{bmatrix} \\ A_k^Q = 1 \\ C_k^{SOC} = \begin{bmatrix} \frac{\partial U_{OC}}{\partial SOC} & -1 \end{bmatrix} \\ C_k^Q = -\frac{i\Delta T}{Q_k^2} \end{cases} \quad (2)$$

The resistance value of the battery increase with the aging process. To realize the model migration of the initial battery model under different aging states, the relationship curve of parameter dynamic change of the initial battery model can be migrated online. Since the migrated initial model relationship curve is a functional relationship with the battery SOC, and the SOC obtained in the estimation process is inaccurate, it is necessary to correct the inaccurate SOC to ensure that the migrated model parameter value is close to the real battery model parameter value. Therefore, in the circuit structure diagram of the migration model shown in Fig. 1, the superscript M is used to represent the parameters of the migrated battery model. The state expression of the dynamic migration model is shown in in Eq. (3).

$$\begin{cases} X = [x_1, x_2, x_3, \dots, x_{10}] \\ SOC_k^M = x_1 SOC_k + x_2 \\ U_{OC,k}^M = x_3 f_{OCV}(SOC_k^M) + x_7 \\ R_{0,k}^M = x_4 f_{R_0}(SOC_k^M) + x_8 \\ R_{p,k}^M = x_5 f_{R_p}(SOC_k^M) + x_9 \\ C_{p,k}^M = x_6 f_{C_p}(SOC_k^M) + x_{10} \\ U_{L,k}^M = U_{OC,k}^M - U_{p,k}^M - IR_{0,k}^M + v_k \end{cases} \quad (3)$$

In the migration model expression Eq. (3), $X = [x_1, x_2, x_3, \dots, x_{10}]$ is the migration factor matrix of the model,

SOC_k^M is the corrected SOC value, $U_{OC}^M, R_0^M, R_p^M, C_p^M$ are the parameter values after migration obtained from the relationship curve between SOC and battery model parameters, U_L^M is the terminal voltage value obtained from the migrated model observation equation.

2.2. *Parameter identification and relation curve extraction of initial model*

It is necessary to obtain the functional relationship between battery parameters and SOC, rather than the specific parameter value at each sampling point in a specific working condition. All parameters in the Thevevin model can be identified offline through the Hybrid Pulse Power Characterization (HPPC) experiment. The process of the HPPC test is shown in Fig. 2.

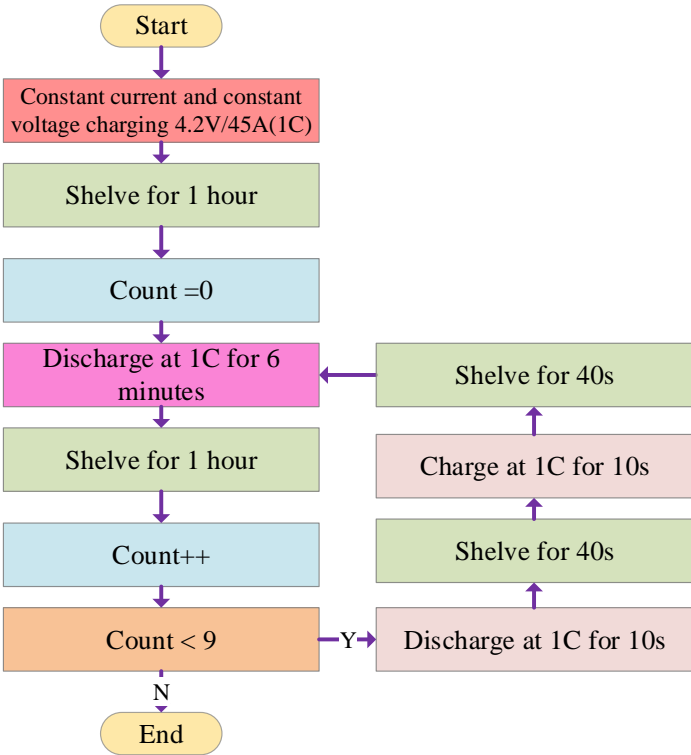


Fig. 2 HPPC experiment step setting

In the process of data analysis and processing, the effective data segment is extracted from the original experimental data, through the analysis of the extracted data segment and the processing method of curve fitting, the relationship between the internal parameters and SOC is obtained, and the accurate construction of the equivalent model is completed, to realize the accurate description of the working characteristics of lithium-ion

battery. Firstly, all voltage data are extracted from the original data to describe the change of battery terminal voltage in the whole process of the HPPC test, as shown in Fig. 3 (a). For the initial Thevenin model, the parameters to be identified are R_0 , R_p , and C_p , which can be identified from the dynamic pulse test stage of the HPPC test, so the data segment of the pulse test in each cycle is extracted. The impulse response curve of lithium-ion battery when SOC is 0.7 is shown in Fig. 3 (b).

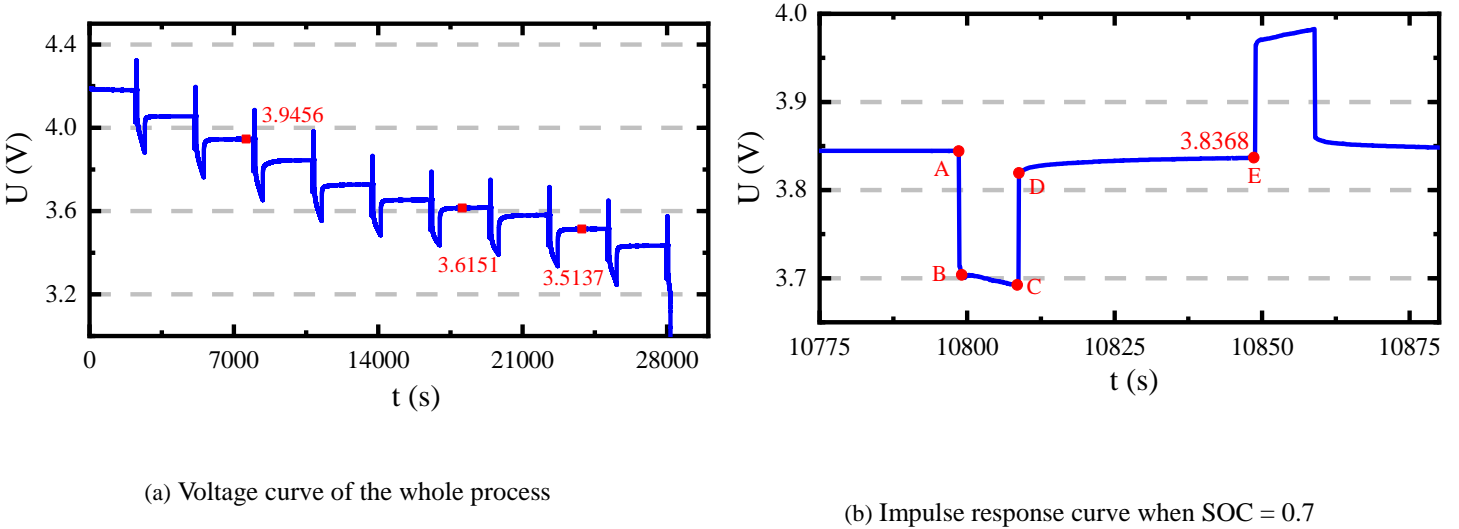


Fig. 3 Voltage response curve of HPPC test

It can be seen from Fig. 3 (a) that after each constant current discharge, the battery is put aside for 1 h, and the voltage gradually tends to be stable, which indicates that the internal chemical reaction and thermal effect have reached a balance. At this time, the battery voltage is its OCV, so the relationship curve between OCV and SOC can be obtained. Fig. 3 (b) reflects the transient and steady-state characteristics of lithium-ion battery. At the beginning of pulse discharge, the battery voltage drops instantaneously, and then the voltage decreases slowly during discharge. At the end of discharge, the battery voltage rebounds immediately, the voltage gradually rises and tends to be stable during shelving. The point-taking calculation method and curve fitting method are used to identify the parameters of pulse test data.

As shown in Fig. 3 (b), the sudden drop of discharge start voltage is the function of R_0 , and the phenomenon of a gradual drop of voltage can be explained by the RC circuit. Therefore, the values of R_0 can be obtained from the

AB segment and CD segment, and the values of R_P and C_P can be obtained from the BC segment and DE segment.

The calculation expression of R_0 is shown in Eq. (4).

$$R_0 = \frac{|\Delta U_{AB}| + |\Delta U_{CD}|}{2I} \quad (4)$$

As shown in Fig. 3 (b), the zero state response curve of the BC segment is selected as the fitting curve segment.

From the KVL relationship of the initial Thevenin model, the circuit expression is shown in Eq. (5).

$$U_L = U_{OC} - IR_0 - IR_p(1 - e^{-\frac{\Delta T}{\tau}}) \quad (5)$$

Eq. (5) is abstracted and its parameterized expression is obtained, as shown in Eq. (6).

$$y = a - b(1 - e^{-\frac{x}{c}}) \quad (6)$$

In Eq. (6), y represents U_L , x represents time t , a , b and c are three parameters corresponding to $U_{OC} - IR_0$, IR_p , and τ in Eq. (5) respectively. The curve fitting method is used to identify the parameters of each stage with SOC from 0.1 to 1.

2.3. Chaotic firefly - particle filtering for SOC and SOH co-estimation

The migration factor matrix is an important parameter to correct the initial battery model and SOC in the online migration process. The determination of migration factor is a nonlinear and non-Gaussian process, so the nonlinear and non-Gaussian PF algorithm is selected to determine it online. Combined with the structural framework and expression of the battery dynamic migration model which is shown in Eq. (3), the migration matrix $X = [x_1, x_2, x_3, \dots, x_{10}]$ is taken as the system state variable, the battery terminal voltage is taken as the system observed measurement, the load current I_k and inaccurate SOC_k in the working process of the battery are taken as the input of the system. The discrete state equation of the system is established, as shown in Eq. (7).

$$\begin{cases} \vec{X}_k = \begin{bmatrix} x_{1,k-1} \\ x_{2,k-1} \\ \dots \\ x_{10,k-1} \end{bmatrix} + \begin{bmatrix} v_1 \\ v_2 \\ \dots \\ v_{10} \end{bmatrix}, \begin{matrix} v_1 \sim N(0, \sigma_1^2) \\ v_2 \sim N(0, \sigma_2^2) \\ \dots \\ v_{10} \sim N(0, \sigma_{10}^2) \end{matrix} \\ U_{L,k} = U_{OC,k} - U_{P,k} - IR_0 + \omega, \omega \sim N(0, \sigma_\omega^2) \end{cases} \quad (7)$$

The initial value of $X = [x_1, x_2, \dots, x_{10}]$ and the variance σ_i^2 of the state value are shown in Tab. 1.

Tab. 1 Dynamic migration model parameter configuration

i	1	2	3	4	5	6	7	8	9	10	ω
$v_{i,0}$	1	0	1	1	1	1	0	0	0	0	<i>null</i>
σ_i^2	0.00001	0.002	0.0001	0.0001	0.0001	0.0001	0.001	0.001	0.001	0.001	0.001

To solve the defects of particle degradation and particle diversity reduction in traditional PF, the intelligent firefly algorithm is introduced. To effectively improve the dependence on the initial solution, slow convergence speed in the later stage, a chaotic algorithm that can map a group of particles to another solution space is added. To sum up, a CF - PF method is proposed. The overall process of the CF - PF method is shown in Fig. 4.

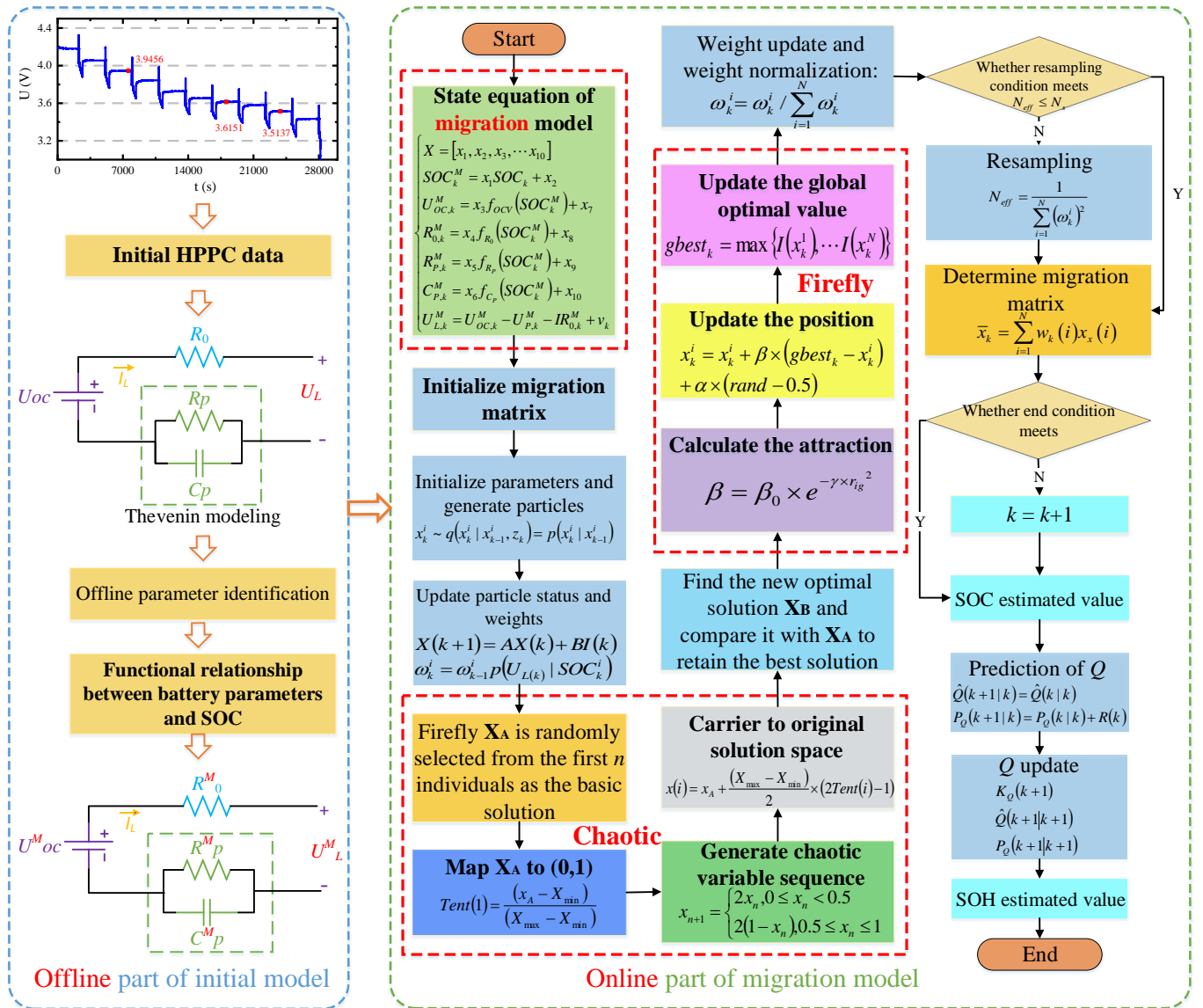


Fig. 4 Overall process of the CF - PF method

In Fig. 4, the complete SOC and SOH co-estimation consists of offline initial modeling and online migration model update. The offline part has been described in Chapters 2.1 and 2.2. The online migration part is based on the PF algorithm, and the parts highlighted in the red box are the improved migration modeling part, the firefly optimization algorithm part, and the chaotic algorithm part, respectively.

2.3.1. Firefly algorithm

Fireflies in nature communicate with others through luminous behavior, but the fluorescence of fireflies is only visible in a certain range. The idea of the firefly algorithm is to initialize the firefly population randomly in the search space. High brightness fireflies attract low brightness fireflies to move towards them, and their positions are both updated at the same time. By moving several times, almost all fireflies concentrate around the brightest firefly, to realize the optimization process. Therefore, the brightness, attraction, and position are several elements of the algorithm. The relative brightness of firefly i to firefly j is shown in Eq. (8).

$$I_{ij} = I_0 \times e^{-\gamma \times r_{ij}^2} \quad (8)$$

In Eq. (8), I_0 is the maximum fluorescence brightness of firefly i . The better the objective function value, the higher the brightness of the firefly itself. For the SOC estimation of lithium-ion batteries in the PF algorithm, the higher the particle weight, the higher its brightness. γ is the light intensity absorption coefficient, which is set to 0.98 in this research. r_{ij} is the spatial distance between fireflies i and j . When this parameter is used in the PF algorithm, it is considered as the estimated value difference between SOC particles. The attraction of firefly i to j is shown in Eq. (9).

$$\beta_{ij} = \beta_0 \times e^{-\gamma \times r_{ij}^2} \quad (9)$$

In Eq. (9), β_0 is the attraction at the light source ($r = 0$), which is the maximum attraction of the light source firefly. The position update of attracted firefly j and global optimal firefly i is shown in Eq. (10).

$$\begin{cases} x_j = x_j + \beta_{ij} \times (x_j - x_i) + \alpha \times (rand - 0.5) \\ x_i = x_i + \alpha \times (rand - 0.5) \end{cases} \quad (10)$$

In Eq. (10), x_i and x_j represent the spatial position of fireflies i and j , which represent the SOC value of particles

1
2 i and j in the PF algorithm. Step factor α is a constant on $[0,1]$, with a value of 0.05. $rand$ is a random factor on
3 $[0,1]$ and obeys uniform distribution. Since other fireflies cannot attract the brightest firefly, the position update
4 equation of the brightest firefly is executed according to the second part in Eq. (10).
5
6

7 2.3.2. *Firefly based on chaotic mapping*

8
9

10 Chaos is a complex nonlinear system dynamic behavior, which uses the characteristics of chaotic motion to
11 improve the optimization efficiency of the algorithm. The basic idea is to linearly map the optimization variables
12 into the chaotic variables through chaotic mapping, and then optimize the search process according to the
13 ergodicity and randomness of chaos. Finally, the obtained solution is linearly transformed into the optimization
14 variable space.
15
16
17
18
19
20
21
22

23 There are many kinds of one-dimensional chaotic mapping functions. At present, the commonly used chaotic
24 functions are Logistic mapping function and Tent chaotic mapping function. Logistic mapping function is a
25 chaotic system, but the speed of searching the optimal solution is affected by the non-uniformity of its function
26 distribution. Tent chaotic mapping function has a higher value taking probability for the Logistic mapping function
27 in the interval $[0, 0.1]$ and $[0.9, 1]$. The distribution of chaotic sequences generated in the interval $[0, 1]$ is more
28 uniform and the iteration speed is faster. So the chaotic sequence of Tent mapping is evenly distributed and has
29 high optimization efficiency. In this research, Tent mapping is used to generate the chaotic sequence, and its
30 mathematical expression is shown in Eq. (11).
31
32
33
34
35
36
37
38
39
40
41
42
43
44

$$45 x_{n+1} = \begin{cases} 2x_n, & 0 \leq x_n < 0.5 \\ 2(1 - x_n), & 0.5 \leq x_n \leq 1 \end{cases} \quad (11)$$

46
47
48

49 Firstly, the initial population with uniform distribution is randomly generated by Tent mapping to ensure the
50 randomness and diversity of the individuals, which is conducive to improving the convergence speed of the
51 algorithm. In the firefly population X_i ($x = 1, 2, \dots, N$) in one iteration, all fireflies are sorted from large to small
52 according to the fluorescence brightness (particle weight), the first 5% of individuals are taken, and the minimum
53 X_{min} and maximum X_{max} of them are obtained as the chaotic search space. A firefly is randomly selected from the
54
55
56
57
58
59
60
61
62
63
64
65

first 5% of individuals, and its spatial position (SOC value) X_A is taken as the basic solution. Eq. (12) is used to map X_A into the (0,1) interval.

$$Tent(1) = \frac{(x_A - X_{min})}{(X_{max} - X_{min})} \quad (12)$$

Eq. (12) is substituted into the Tent map of Eq. (11), the chaotic variable sequence $Tent(m)$ ($m = 1, 2, \dots, ITER_{max}$) is generated iteratively, and $ITER_{max}$ is the maximum number of iterations of chaotic search, which is set to 200.

The generated sequence $Tent(m)$ is carried to the original solution space to generate $x(m)$ by Eq. (13).

$$x(m) = x_A + \frac{(X_{max} - X_{min})}{2} \times 2(Tent(m) - 1) \quad (13)$$

The fluorescence brightness (particle weight) of each firefly in the new sequence $x(m)$ is calculated one by one to generate a new optimal solution X_B , which is compared with the particle weight of X_A to retain the best solution and make the algorithm jump out of the local optimum.

2.3.3. SOC and SOH co-estimation based on dual filter

In this research, the combination of the PF algorithm and EKF algorithm is used to realize the SOC and SOH co-estimation of lithium-ion batteries. After the SOC value at the current time is estimated by CF - PF algorithm, this value is used as the input of the SOH estimation filter at the current time to correct the a priori capacity Q obtained from the state transition equation in Eq. (1). After the Q at the current time is obtained, it is used as the input of CF - PF to correct the SOC at the next time by updating the coefficient matrix B in the state transition equation. In the separate estimation of SOC, the Q in matrix B is the calibrated capacity value, which does not change with the increase in the number of iterations. In the co-estimation, Q is inversely updated and corrected to realize the mutual promotion and influence of the two state parameters. The principle of SOC and SOH mutual correction through the dual filter is shown in Fig. 5.

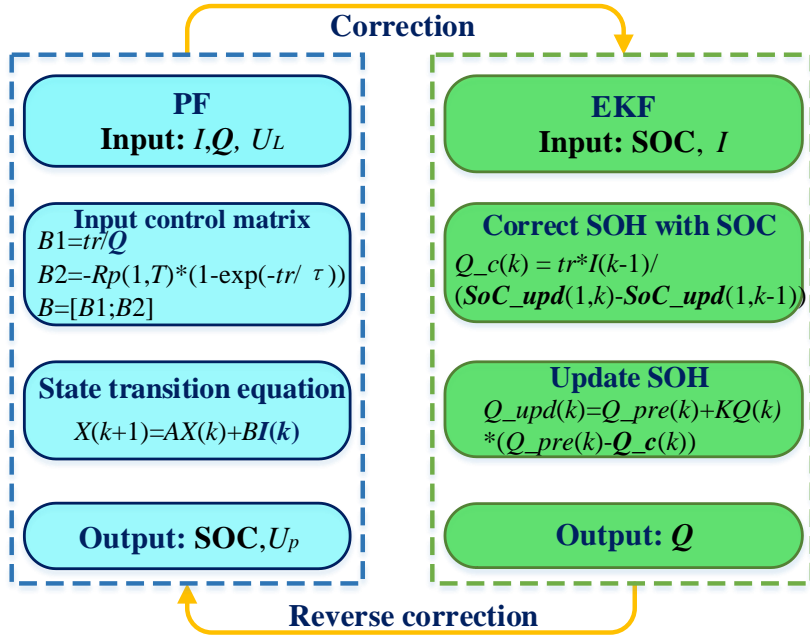


Fig. 5 Mutual correction of SOC and SOH

3. Experimental analysis

3.1. Experimental platform construction

The ternary lithium-ion battery with a rated capacity of 45Ah and a nominal voltage of 3.7 V is used for the experimental test. A BTS200-100-104 battery test equipment is used as the test platform, and a software that is installed at the PC control terminal is used to control the battery charging and discharging conditions as to match with the test equipment. To avoid the influence of temperature inconsistency on the parameters and OCV of the battery, all the experiments in this research are carried out at constant temperature of 25 °C. The experimental platform established in this research is shown in Fig. 6.

1
2
3
4
5
6
7
8
9
10
11
12
13
14
15
16
17
18
19
20
21
22
23
24
25
26
27
28
29
30
31
32
33
34
35
36
37
38
39
40
41
42
43
44
45
46
47
48
49
50
51
52
53
54
55
56
57
58
59
60
61
62
63
64
65

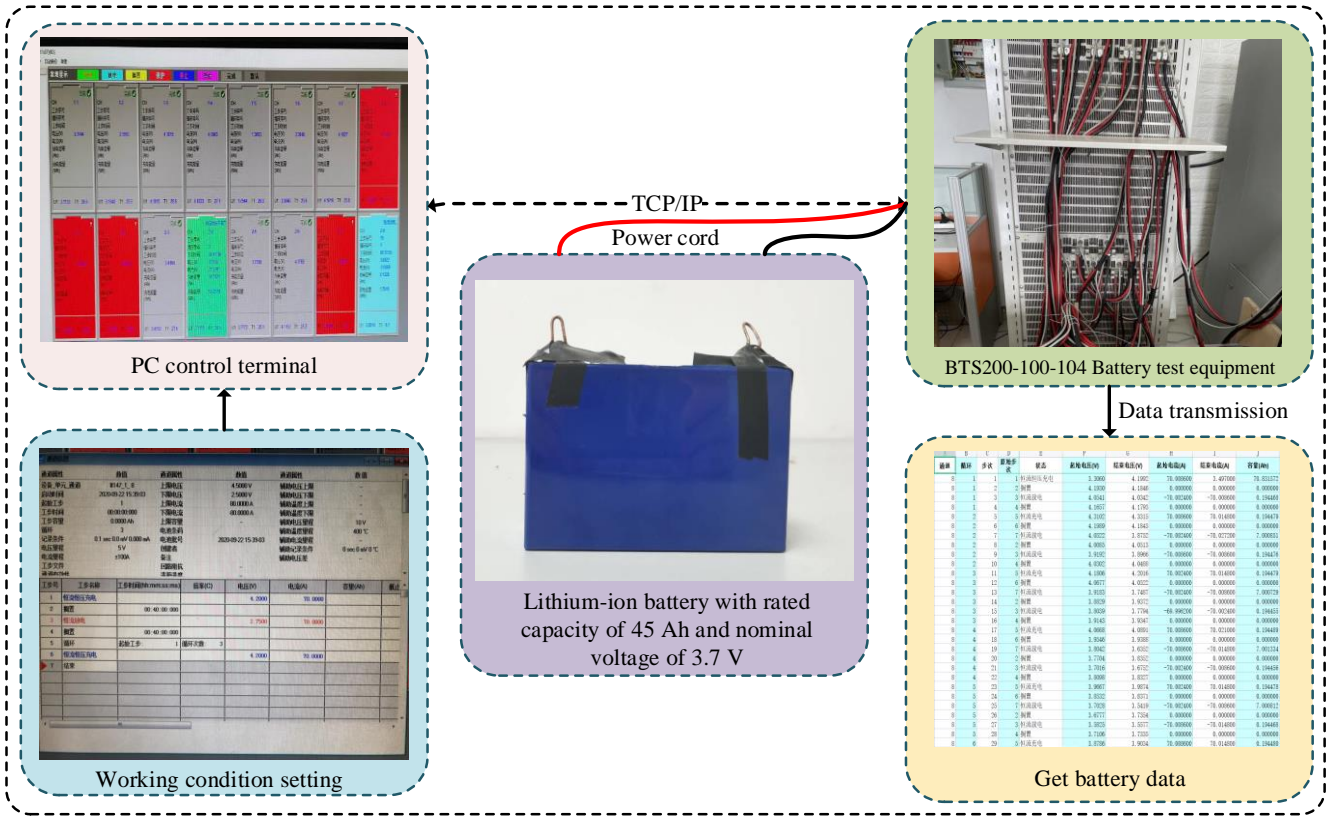


Fig. 6 Experimental platform construction

3.2. Accuracy verification of dynamic migration model

In Chapter 2.2, the parameters of each stage from 0.1 to 1 of SOC are identified by curve fitting. The obtained offline parameter identification results of R_0 , R_p , and C_p are shown in Tab. 2.

Tab. 2 Offline parameter identification results

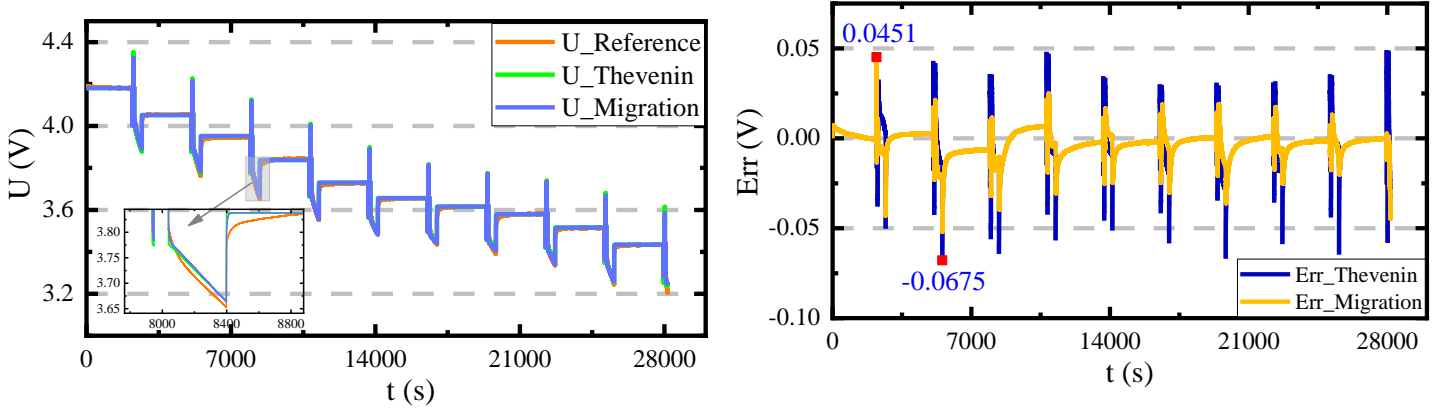
SOC	R_0/Ω	R_p/Ω	$C_p/\mu F$
1	0.0028	0.0005752	14361.9611
0.9	0.0032	0.0006374	11909.3191
0.8	0.0028	0.0006786	11497.2001
0.7	0.0024	0.0007104	11392.1734
0.6	0.0032	0.0006286	11800.8272
0.5	0.0013	0.0004946	17270.5216
0.4	0.0022	0.0004876	17518.4578
0.3	0.0037	0.0005244	17080.4729
0.2	0.0034	0.000601	15094.8419
0.1	0.0029	0.0008518	9839.16412

The expression of the relationship between the three parameters and the dynamic change of SOC is shown in

Eq. (14).

$$\begin{cases} R_0 = -0.02978x^6 + 0.09091x^5 - 0.105x^4 + 0.05578x^3 - 0.01196x^2 + 0.0001415x + 0.003219 \\ R_p = 0.06207x^6 - 0.189x^5 + 0.2216x^4 - 0.1317x^3 + 0.04575x^2 - 0.009677x + 0.001471 \\ C_p = -1.165e + 07x^6 + 3.262e + 07x^5 - 3.33e + 07x^4 + 1.529e + 07x^3 - 3.355e + 06x^2 + 4.429e + 05x + 2617 \end{cases} \quad (14)$$

The obtained OCV-SOC relationship curve and the relational expression between parameters and SOC are used for the dynamic migration process in the migration model. To verify the accuracy of the improved migration model compared with the ordinary Thevenin model, the two models are verified under HPPC working condition. The current I is taken as the input value, and the terminal voltage output by the model and the actual terminal voltage data of lithium-ion battery under the same input current are obtained respectively. The experimental verification results are shown in Fig. 7.



(a) Terminal voltage comparison

(b) Terminal voltage error

Fig. 7 Comparison of output terminal voltage under HPPC working condition

As can be seen from Fig. 7 (b), the output voltage error of the migration model is significantly smaller than that of the Thevenin model during the whole charge and discharge process. The maximum output error of the Thevenin model is as high as 0.0675 V, and the output error of the migration model is only 0.0451 V. It proves that the migration model can more accurately describe the dynamic characteristics of the battery, which is greatly improved compared with the traditional model. The application of the migration model lays a solid foundation for

better completing the SOC and SOH co-estimation of lithium-ion batteries.

3.3. Co-estimation verification under HPPC test

Based on the application of the battery migration model, the experimental verification of SOC and SOH co-estimation of the proposed novel CF - PF algorithm under HPPC working condition is carried out. In the SOH estimation, the reference value 99.11% is obtained through rigorous capacity calibration experiment. After the battery is fully charged and discharged for three times, the average discharge capacity of the three times is the actual capacity under the current state, and then the current SOH is obtained. The co-estimation results of the traditional PF algorithm, firefly - particle filtering (F - PF) algorithm, and CF - PF algorithm under HPPC working condition are shown in Fig. 8.

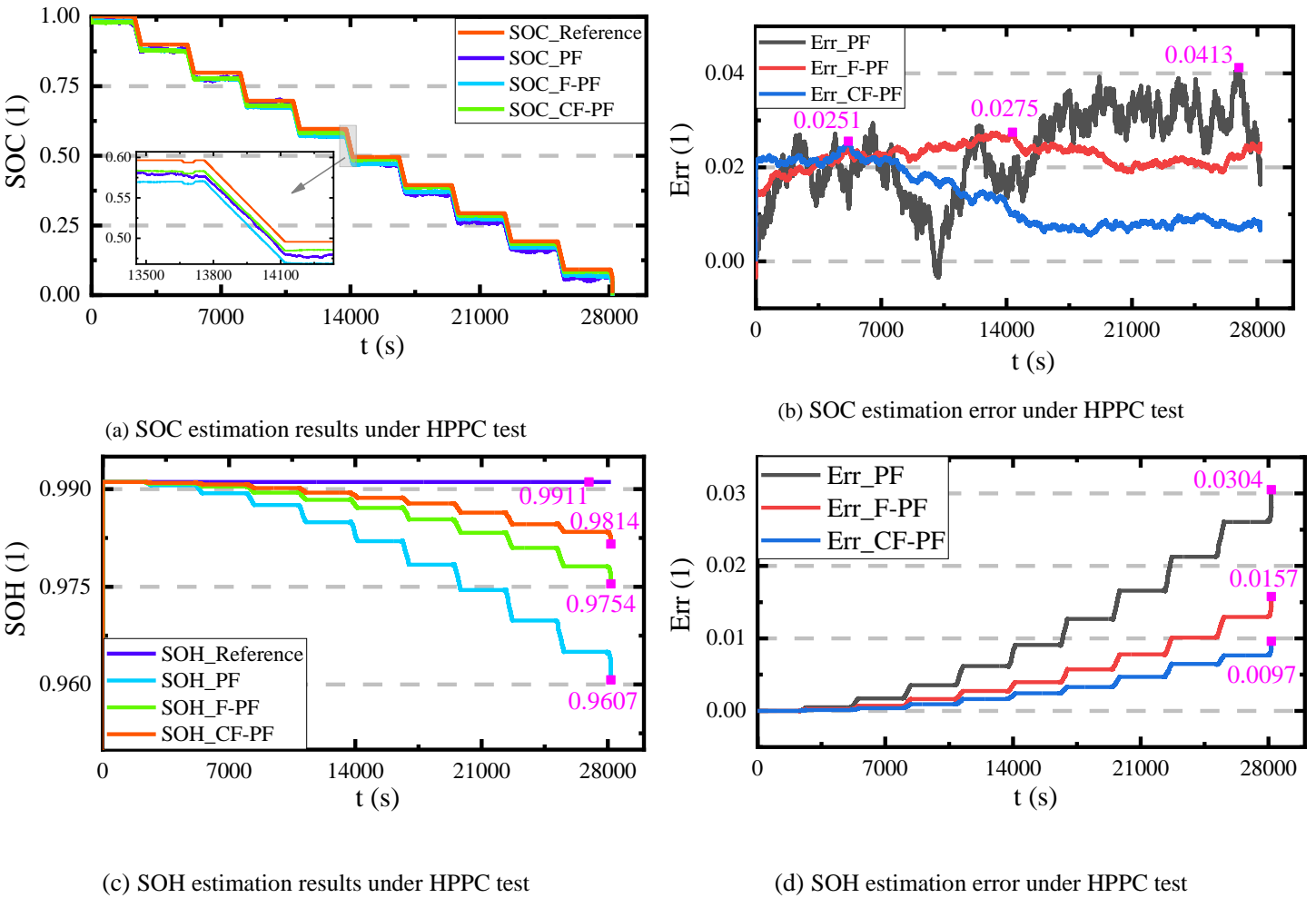


Fig. 8 Comparison of SOC and SOH co-estimation under HPPC test

As can be seen from Fig. 8 (b), the SOC estimation error of the traditional PF algorithm fluctuates greatly and is very unstable. The divergence in the later stage is serious, and the maximum error is as high as 4.13%. The stability of the F - PF algorithm is significantly improved, the error in the later stage is stable and has slight divergence, the maximum error is 2.75%, which proves that the added firefly algorithm is effective to improve particle optimization ability and greatly improve the overall SOC estimation accuracy. The accuracy of the CF - PF algorithm is greatly improved on the whole, and the algorithm has an obvious convergence effect and high stability in the later stage. The maximum SOC estimation error is only 2.51%. The added chaotic algorithm improves the estimation accuracy again based on the firefly algorithm and improves the defects that the firefly algorithm is easy to fall into local optimization, early maturity, and divergence in the later stage. As can be seen from Fig. 8 (c) and Fig. 8 (d), both the firefly algorithm and chaotic algorithm show obvious improvement effects. The maximum error of the PF algorithm is 3.04%, that of the F - PF algorithm is 1.57%, and that of the CF - PF algorithm is 0.97%. CF - PF algorithm shows effective improvement of convergence and accuracy. The three algorithms are compared through three evaluation indexes: maximum error, mean absolute error (MAE), and root-mean-square error (RMSE). The comparison of SOC and SOH co-estimation results under the HPPC test is shown in Tab. 3.

Tab. 3 Comparison of SOC and SOH co-estimation results under HPPC test

Estimation method	PF	F - PF	CF - PF
Maximum Error (SOC)	4.13%	2.75%	2.51%
MAE (SOC)	2.32%	2.22%	1.34%
RMSE (SOC)	2.48%	2.24%	1.48%
Maximum Error (SOH)	3.04%	1.57%	0.97%
MAE (SOH)	0.99%	0.47%	0.28%
RMSE (SOH)	1.32%	0.63%	0.38%

3.4. Co-estimation verification under BBDST test

The working conditions of electric vehicles in actual operation are dynamic, irregular, complex, and changeable.

To better simulate the actual operation, the ternary lithium-ion battery is tested by setting the working condition experiment concerning the Beijing bus dynamic stress test (BBDST). BBDST is the working condition obtained from the real data collection of Beijing buses, including not only the basic working conditions such as starting, braking, and stopping, but also the operations such as acceleration, taxiing, and rapid acceleration. The co-estimation results of the traditional PF algorithm, F - PF algorithm, and CF - PF algorithm under BBDST working condition are shown in Fig. 9.

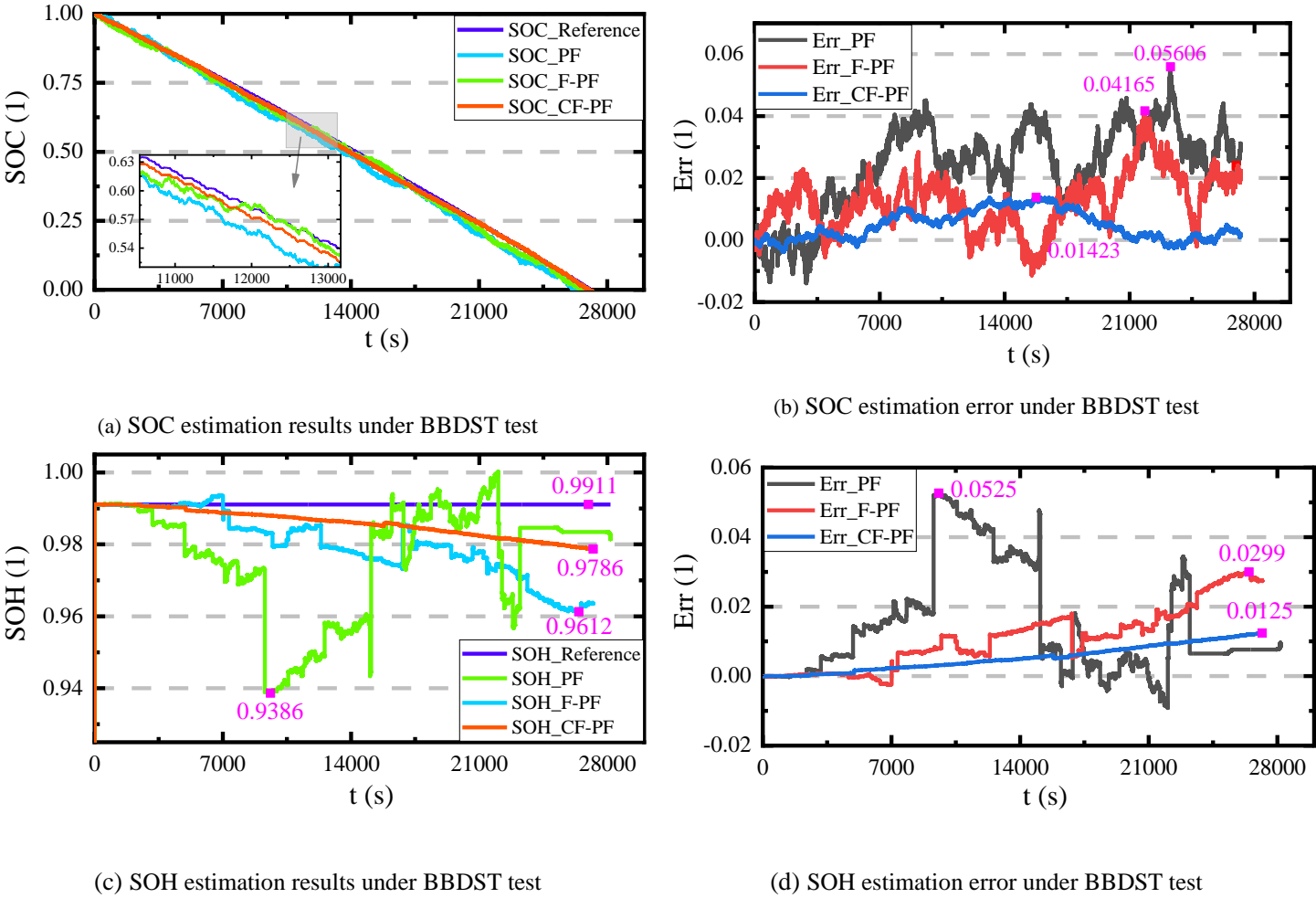
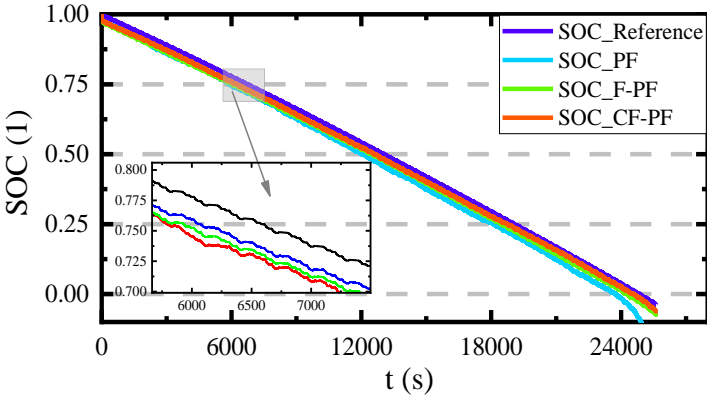


Fig. 9 Comparison of SOC and SOH co-estimation under BBDST test

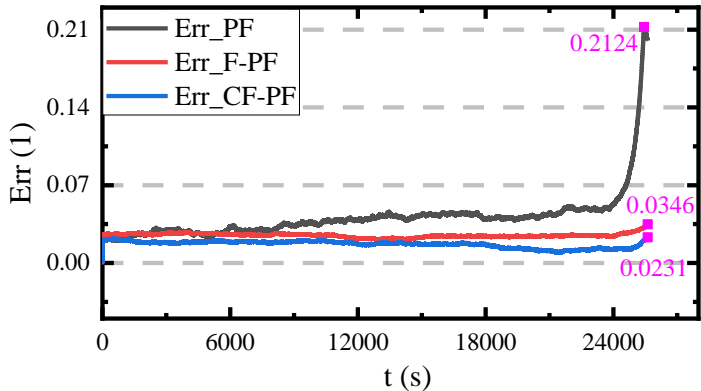
As can be seen from Fig. 9 (b), the SOC estimation error of the PF algorithm fluctuates greatly and is extremely unstable, the maximum error is as high as 5.60%. The F-PF algorithm improves the overall estimation accuracy to a certain extent, with a maximum error of 4.16%. With the addition of the chaotic algorithm, the performance

of the CF - PF algorithm is greatly improved as a whole. It can maintain high stability even under the complex and changeable BBDST working condition. The algorithm can converge in the later stage, fluctuate around 0, and the maximum error is only 1.42%. As can be seen from Fig. 9 (c) and Fig. 9 (d), the stability of SOH estimation of the traditional PF algorithm is poor. There is a large fluctuation in the medium term, and the maximum error can reach 5.25%. There is also an obvious fluctuation in the later stage. The stability and accuracy of the F - PF algorithm are both improved obviously, but it is still highly divergent, and the maximum error is only 2.99%. CF - PF algorithm has a good performance in the whole BBDST working condition. The stability of the algorithm is very strong, the estimation results do not fluctuate greatly, and the maximum error is only 1.25%.

The above experimental verification are carried out under the battery condition of high health. To verify the universality of the algorithm and its ability to correct the battery state estimation under severe aging, BBDST experiment is conducted on the battery with a SOH of 91.31% after 278 cycles of charging and discharging. The data under this working condition are used for algorithm and model verification, the results are shown in Fig. 10.

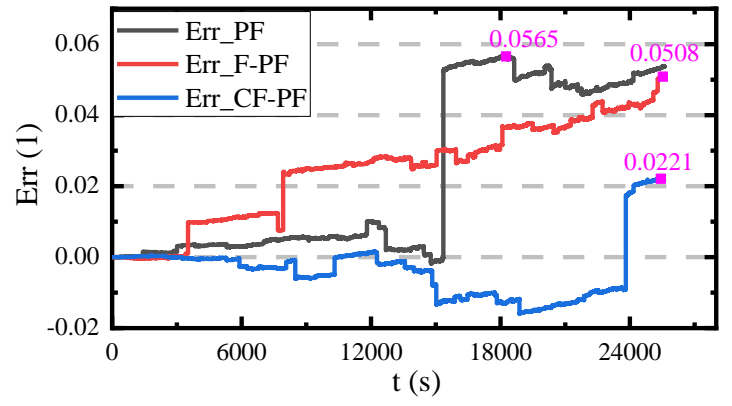
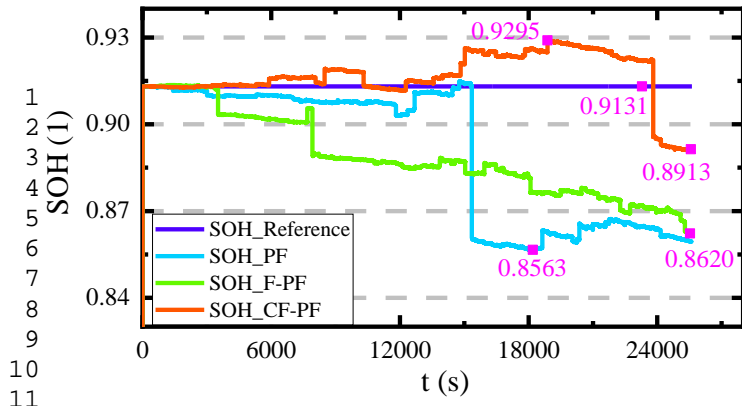


(a) SOC estimation results under BBDST test and severe aging



(b) SOC estimation error under BBDST test and severe aging

1
2
3
4
5
6
7
8
9
10
11
12
13
14
15
16
17
18
19
20
21
22
23
24
25
26
27
28
29
30
31
32
33
34
35
36
37
38
39
40
41
42
43
44
45
46
47
48
49
50
51
52
53
54
55
56
57
58
59
60
61
62
63
64
65



(c) SOH estimation results under BBDST test and severe aging

(d) SOH estimation error under BBDST test and severe aging

Fig. 10 Comparison of SOC and SOH co-estimation under BBDST test and severe aging

As can be seen from Fig. 10 (b), although the stability of the three algorithms is high in the early stage, PF is seriously divergent at the end of the discharge, and the error increases rapidly, which is not within the acceptable range. The estimation error of F - PF and CF - PF have high stability, and the overall accuracy of CF - PF is relatively high. The maximum error of F - PF is 3.46%, and that of CF - PF is only 2.31%. As can be seen from Fig. 10 (c) and Fig. 10 (d), the traditional PF has a large error in SOH estimation, the estimation results are unreliable. F - PF makes some improvements to increase its estimation reliability, but it is still not within the acceptable range. The SOH estimation result of CF - PF algorithm has small fluctuation and high accuracy, the error can be controlled within 2.21%. Although the overall effect of co-estimation under severe aging is relatively poor compared with that under high SOH, the CF - PF algorithm proposed in this research still has a very obvious effect on improving the co-estimation accuracy.

The three algorithms are compared through three evaluation indexes: maximum error, MAE, and RMSE. The comparison of SOC and SOH co-estimation results under the BBDST test is shown in Tab. 4.

Tab. 4 Comparison of SOC and SOH co-estimation results under BBDST test

Estimation method	PF	F - PF	CF - PF
Maximum Error (SOC)	5.60%	4.16%	1.42%
MAE (SOC)	2.48%	1.31%	0.52%
RMSE (SOC)	2.76%	1.54%	0.67%

Maximum Error (SOH)	5.25%	2.99%	1.25%
MAE (SOH)	1.52%	1.10%	0.52%
RMSE (SOH)	2.16%	1.40%	0.63%
Maximum Error (SOC/ severe aging)	21.24%	3.46%	2.31%
MAE (SOC/ severe aging)	5.76%	3.08%	2.09%
RMSE (SOC/ severe aging)	6.03%	3.13%	2.18%
Maximum Error (SOH/ severe aging)	5.65%	5.08%	2.21%
MAE (SOH/ severe aging)	3.44%	3.32%	1.13%
RMSE (SOH/ severe aging)	3.82%	3.69%	1.26%

4. Conclusions

In this research, to achieve high-precision real-time state-of-charge and state-of-health co-estimation of lithium-ion batteries, to provide more accurate residual battery power for new energy vehicle drivers that can better predict the remaining mileage thereby ensuring safe driving, a novel dynamic migration model and a chaotic firefly-particle filtering method are proposed. Under complex working condition, the root-mean-square error of state-of-charge and state-of-health estimation of chaotic firefly - particle filtering method is 0.67% and 0.63% respectively, which are improved by 2.09% and 1.53% compared with the traditional particle filtering algorithm.

In summary, the proposed model and method plays an obvious and effective role in improving the state-of-charge and state-of-health co-estimation accuracy of lithium-ion batteries. This study provides a theoretical basis for the battery condition monitoring, and in the practical application of new energy vehicles, it has an important contribution to real-time monitoring of vehicle status in ensuring safe driving for drivers. However, in the actual driving process, the temperature is complex and changeable, and the influence of temperature on the battery state estimation has not been considered in this study, which is also the research direction in the future.

Acknowledgments

The work is supported by the National Natural Science Foundation of China (No. 62173281, 61801407), Sichuan science and technology program (No. 2019YFG0427), China Scholarship Council (No. 201908515099), and Fund of Robot Technology Used for Special Environment Key Laboratory of Sichuan Province (No. 18kftk03).

References

1. Aung, H., et al., *Battery Management System With State-of-Charge and Opportunistic State-of-Health for a Miniaturized Satellite*. Ieee Transactions on Aerospace and Electronic Systems, 2020. **56**(4): p. 2978-2989.
2. Zhu, F. and J. Fu, *A Novel State-of-Health Estimation for Lithium-Ion Battery via Unscented Kalman Filter and Improved Unscented Particle Filter*. Ieee Sensors Journal, 2021. **21**(22): p. 25449-25456.
3. Bian, X., et al., *State-of-Health Estimation of Lithium-Ion Batteries by Fusing an Open Circuit Voltage Model and Incremental Capacity Analysis*. Ieee Transactions on Power Electronics, 2022. **37**(2): p. 2226-2236.
4. Cen, Z. and P. Kubiak, *Lithium-ion battery SOC/SOH adaptive estimation via simplified single particle model*. International Journal of Energy Research, 2020. **44**(15): p. 12444-12459.
5. Feng, Y., et al., *Robust Estimation for State-of-Charge and State-of-Health of Lithium-Ion Batteries Using Integral-Type Terminal Sliding-Mode Observers*. Ieee Transactions on Industrial Electronics, 2020. **67**(5): p. 4013-4023.
6. Gao, Y., et al., *Co-Estimation of State-of-Charge and State-of-Health for Lithium-Ion Batteries Using an Enhanced Electrochemical Model*. Ieee Transactions on Industrial Electronics, 2022. **69**(3): p. 2684-2696.
7. Gholizadeh, M. and A. Yazdizadeh, *Systematic mixed adaptive observer and EKF approach to estimate SOC and SOH of lithium-ion battery*. Iet Electrical Systems in Transportation, 2020. **10**(2): p. 135-143.
8. Goud, J.S., R. Kalpana, and B. Singh, *An Online Method of Estimating State of Health of a Li-Ion Battery*. Ieee Transactions on Energy Conversion, 2021. **36**(1): p. 111-119.
9. Hashemi, S.R., A.M. Mahajan, and S. Farhad, *Online estimation of battery model parameters and state of health in electric and hybrid aircraft application*. Energy, 2021. **229**: p. 1-13.
10. Hein, T., et al., *A capacity-based equalization method for aged lithium-ion batteries in electric vehicles*. Electric Power Systems Research, 2021. **191**: p. 1-15.
11. Hu, X., et al., *An enhanced multi-state estimation hierarchy for advanced lithium-ion battery management*. Applied Energy, 2020. **257**: p. 1-14.
12. Kawahara, Y., et al., *Development of status detection method of lithium-ion rechargeable battery for hybrid electric vehicles*. Journal of Power Sources, 2021. **481**: p. 1-18.
13. Khaki, B. and P. Das, *Voltage loss and capacity fade reduction in vanadium redox battery by electrolyte flow control*. Electrochimica Acta, 2022. **405**: p. 1-10.
14. Wu, J.J., et al., *A multi-scale fractional-order dual unscented Kalman filter based parameter and state of charge joint estimation method of lithium-ion battery*. Journal of Energy Storage, 2022. **50**: p. 1-17.
15. Kim, J., L. Krueger, and J. Kowal, *On-line state-of-health estimation of Lithium-ion battery cells using frequency excitation*. Journal of Energy Storage, 2020. **32**: p. 1-12.
16. Lai, X., et al., *Parameter sensitivity analysis and simplification of equivalent circuit model for the state of charge of lithium-ion batteries*. Electrochimica Acta, 2020. **330**: p. 1-14.
17. Li, J., et al., *Joint estimation of state of charge and state of health for lithium-ion battery based on dual adaptive extended Kalman filter*. International Journal of Energy Research, 2021. **45**(9): p. 13307-13322.
18. Liu, B., X. Tang, and F. Gao, *Joint estimation of battery state-of-charge and state-of-health based on a simplified pseudo-two-dimensional model*. Electrochimica Acta, 2020. **344**: p. 1-14.
19. Ma, Y., et al., *State of charge and state of health estimation based on dual nonlinear adaptive observer and hysteresis model of lithium-ion battery*. Journal of Renewable and Sustainable Energy, 2021. **13**(4): p. 1-9.
20. Maleki, S., B. Ray, and M. Hagh, *Hybrid framework for predicting and forecasting State of Health of Lithium-ion batteries in Electric Vehicles*. Sustainable Energy Grids & Networks, 2022. **30**: p. 1-14.
21. Naha, A., et al., *An Incremental Voltage Difference Based Technique for Online State of Health Estimation of Li-ion Batteries*. Scientific Reports, 2020. **10**(1): p. 1-10.
22. Ning, J., et al., *A rapid detection method for the battery state of health*. Measurement, 2022. **189**: p. 1-8.
23. Park, J., et al., *Complementary cooperative SOC/capacity estimator based on the discrete variational derivative*

combined with the DEKF for electric power applications. *Energy*, 2021. **232**: p. 1-9.

24. Ren, P., et al., *Fusion estimation strategy based on dual adaptive Kalman filtering algorithm for the state of charge and state of health of hybrid electric vehicle Li-ion batteries*. *International Journal of Energy Research*, 2022. **46**(6): p. 7374-7388.
25. Sabet, P.S., G. Stahl, and D.U. Sauer, *Non-invasive investigation of predominant processes in the impedance spectra of high energy lithium-ion batteries with nickel-cobalt-aluminum cathodes*. *Journal of Power Sources*, 2020. **472**: p. 1-8.
26. Sakile, R. and U.K. Sinha, *Estimation of State of Charge and State of Health of Lithium-Ion Batteries Based on a New Adaptive Nonlinear Observer*. *Advanced Theory and Simulations*, 2021. **4**(11): p. 1-13.
27. Shi, G., et al., *Determination of Optimal Indicators Based on Statistical Analysis for the State of Health Estimation of a Lithium-Ion Battery*. *Frontiers in Energy Research*, 2021. **9**: p. 1-7.
28. Shi, N., et al., *State-of-charge estimation for the lithium-ion battery based on adaptive extended Kalman filter using improved parameter identification*. *Journal of Energy Storage*, 2022. **45**: p. 1-10.
29. Sun, H., et al., *State-of-health estimation of retired lithium-ion battery module aged at 1C-rate*. *Journal of Energy Storage*, 2022. **50**: p. 1-13.
30. Tan, X., et al., *Online state-of-health estimation of lithium-ion battery based on dynamic parameter identification at multi timescale and support vector regression*. *Journal of Power Sources*, 2021. **484**: p. 1-10.
31. Tran, M.-K., et al., *A comprehensive equivalent circuit model for lithium-ion batteries, incorporating the effects of state of health, state of charge, and temperature on model parameters*. *Journal of Energy Storage*, 2021. **43**: p. 1-8.
32. Wang, Z., et al., *A review on online state of charge and state of health estimation for lithium-ion batteries in electric vehicles*. *Energy Reports*, 2021. **7**: p. 5141-5161.
33. Wu, T., et al., *SOC and SOH Joint Estimation of Lithium-Ion Battery Based on Improved Particle Filter Algorithm*. *Journal of Electrical Engineering & Technology*, 2022. **17**(1): p. 307-317.
34. Xia, Z. and J.A. Abu Qahouq, *State-of-Charge Balancing of Lithium-Ion Batteries With State-of-Health Awareness Capability*. *Ieee Transactions on Industry Applications*, 2021. **57**(1): p. 673-684.
35. Xiao, D., et al., *Reduced-Coupling Coestimation of SOC and SOH for Lithium-Ion Batteries Based on Convex Optimization*. *Ieee Transactions on Power Electronics*, 2020. **35**(11): p. 12332-12346.
36. Xu, Z., et al., *Co-estimating the state of charge and health of lithium batteries through combining a minimalist electrochemical model and an equivalent circuit model*. *Energy*, 2022. **240**: p. 1-17.
37. Yan, N., et al., *Research on energy management and control method of microgrid considering health status of batteries in echelon utilization*. *Energy Reports*, 2021. **7**: p. 389-395.
38. Zhang, Q., et al., *Fractional calculus based modeling of open circuit voltage of lithium-ion batteries for electric vehicles*. *Journal of Energy Storage*, 2020. **27**: p. 1-12.
39. Ling, L., et al., *State of charge estimation of Lithium-ion batteries based on the probabilistic fusion of two kinds of cubature Kalman filters*. *Journal of Energy Storage*, 2021. **43**: p. 1-9.
40. Han, Q.N., F. Jiang, and Z. Cheng, *The State of Health Estimation Framework for Lithium-Ion Batteries Based on Health Feature Extraction and Construction of Mixed Model*. *Journal of the Electrochemical Society*, 2021. **168**(7): p. 1-19.
41. Shan, H.P., et al., *An efficient and independent modeling method for lithium-ion battery degradation*. *Ionics*, 2022. **28**(1): p. 99-105.
42. Qian, K.F. and X.T. Liu, *Hybrid optimization strategy for lithium-ion battery's State of Charge/Health using joint of dual Kalman filter and Modified Sine-cosine Algorithm*. *Journal of Energy Storage*, 2021. **44**: p. 1-6.
43. Hashemi, S.R., A.M. Mahajan, and S. Farhad, *Online estimation of battery model parameters and state of health in electric and hybrid aircraft application*. *Energy*, 2021. **229**: p. 1-16.